The Physics of Knocking Over LEGO Minifigures With

Time Reversal Focused Vibrations

Lucas A. Barnes

A senior thesis submitted to the faculty of
Brigham Young University
In partial fulfillment of the requirements for the degree of

Bachelor of Science

Brian E. Anderson, Advisor

Department of Physics and Astronomy

Brigham Young University

April 2021

ABSTRACT

The Physics of Knocking Over LEGO Minifigures With
Time Reversal Focused Vibrations

Lucas A. Barnes
Department of Physics and Astronomy
Bachelor of Science

Time reversal (TR) is a method of focusing wave energy at a point in space. The optimization of a TR demonstration is described that is designed to knock over only one selected LEGO minifigure among other minifigures by focusing vibrations within an aluminum plate at the target minifigure. The goal is to achieve high repeatability of the demonstration along with reducing the cost of the demonstration. By comparing the motion of the minifigure and the plate directly beneath its feet, it is determined that a major factor inhibiting the repeatability of the demonstration is that smaller vibrations leading up to the focal event cause the minifigure to bounce repeatedly, losing contact with the plate and ending up in the air during the main focal event intended to knock over the minifigure. The effects of amplitude, frequency, TR technique, plate thickness, and vibration sensor type are explored to determine their impact on the repeatability of the demonstration. A description is given of the implementation of the demonstration for a museum exhibit. This demonstration illustrates the power of TR focusing and the principles learned by optimizing this demonstration can be applied to other real-world applications.

Keywords: time reversal; acoustics; vibrations; focusing; demonstration

Acknowledgments

Table of Contents

List of Figures

List of Tables

1 Introduction

Time Reversal (TR) is a wave focusing method that can be used to achieve spatial focusing.[1-3] The process involves reversing an impulse response obtained between two points in space and emitting it from one of these locations so that the waves constructively interfere at the other location. In fact, the time-reversed impulse response (TRIR) may be emitted from either location and the same focusing signal will result at the other location due to acoustic reciprocity in a linear, time-invariant environment.

TR was originally named matched signal processing and was developed for underwater acoustic applications.[4,5] During the traditional TR process, waves sent through the system are affected by the transfer function of the system during the forward step (when the impulse response is obtained) and again during backward step (the broadcast of the TRIR). This double filtering of the system (the matched signal process) decreases the spatial resolution of the TR focusing and introduces relatively high temporal side lobes compared to the focus peak, which both reduce the quality of a focus. One solution to this issue is a time reversal method called inverse filtering or deconvolution TR,[6-9] which compensates for the forward step transfer function prior to the backward step. This provides improved spatial and temporal confinement when the TR focusing is impulsive in nature, but at the cost of a reduced TR focusing amplitude.

Some general uses of TR include energy focusing, secure communications, and source imaging. As an example of energy focusing, TR has been used to focus ultrasonic waves to the location of kidney stones in order to break them into smaller pieces non-intrusively.[10,11] In

communications applications, TR is used to send a private message that would only be discernable at the target location, whereas elsewhere it would just sound like noise.[4,12-15] TR can also be used to image earthquakes[16-19] and aero-acoustic sources[20-22] by modeling the propagation of time-reversed recordings. TR has been used in nondestructive evaluation applications to focus energy to various points of interest in order to locally quantify the nonlinear response of those points, which allows cracks and defects to be imaged since they are the sources of that nonlinear response.[3,23-25]

One demonstration of TR acoustics was presented by Fink *et al.*[26] in 1999. In their demonstration, they used an array of loudspeakers and microphones called a time reversal mirror to record sounds, reverse them, and then focus the reversed sounds back to their source. If a person stood in front of the array and said "hello", the time reversal mirror would focus the sound as "olleh" back to the person's mouth where the sound originated. The authors stress in the paper that the sound is not just being retransmitted to spread out into the room like normal sound, and that it instead converges only at the person's mouth via constructive interference of waves generated by the loudspeaker array and by the virtual array made up of appropriately timed reflections from the room boundaries.

In another demonstration by de Mello *et al.*,[27] TR was used to focus surface water waves in a tank. The border of the tank was lined with 148 transducers that could record incoming waves and then emit reversed recordings of them. For their TR experiments, first an object was dropped into the tank as an impulsive source of surface waves. The transducers recorded the reflections of the waves off the sides of the tank and then, after the water had settled, the reversed recordings were broadcast, causing the waves to converge at the original source location and create a focused motion of the surface that was clearly visible to observers.

2

More recently, Heaton *et al.*[28] developed a visual demonstration of TR focused vibrations in a thin plate. A single vibration speaker, or shaker, was used to excite vibrations in the plate after which a scanning laser Doppler vibrometer (SLDV) was used to quantify reverberation time and vibration coupling efficiency from the shaker to plates. Various plate materials were tested to explore the possible spatial confinement of the TR focus as well as the highest focal amplitude possible in different plates. They found that glass, while fragile, provided the highest coupling efficiency and focal amplitude at the lowest cost, while aluminum provided results that were nearly as good while being much more durable. In order to demonstrate the focusing visually, salt was distributed on the plate. Using a slow-motion camera, observers could then see the salt thrown off the plate at the location and time of the focus, while the salt elsewhere on the plate stayed mostly in contact with the plate during the focus. Additionally, some small objects like cardboard cylinders, wooden corks, and LEGO minifigures could be placed at the focal location and knocked over (fall onto its side) during the focus, but not knocked over when placed away from the focal location. However, the ability to knock over the target object was not repeatable enough to use for consistent demonstration (this is known because author BEA was a coauthor on the work of Heaton *et al.*). Their work focused mainly on achieving the highest possible focal amplitude for the purpose of creating a visual demonstration of TR focusing but they did not optimize the repeatability of knocking over small objects at the focal location. This resulted in a very loud and shrill sounding demonstration that sometimes launched an object such as a minifigure several centimeters into the air before falling over and sometimes only made the object rattle on top of the plate, but it would remain standing.

This paper expands on the results of Heaton *et al.* to create a more repeatable, interactive, user-friendly demonstration of TR focusing for a museum exhibit. Because the demonstration

would be in an exhibition hall, reducing the audible noise of the demonstration was also a goal. A 100% reliable means of knocking over a target LEGO minifigure while leaving surrounding minifigures standing is determined in this work by utilizing the TR inverse filter (or deconvolution) method at an optimal excitation level from multiple shakers. Previously, the repeatability of knocking over a target LEGO minifigure with TR acoustics in a thin aluminum plate was around 30%, not previously reported by Heaton *et al.* An explanation is given here for why the target minifigure might not be knocked over despite a sufficiently large TR focal amplitude. The work of Heaton *et al.* focused on obtaining the largest possible peak focal amplitude through the use of clipping TR (a variant of one-bit TR[29,30]), whereas here it is shown that the higher temporal quality of the TR focusing obtained with deconvolution TR is critical to the successful repeatability of this demonstration. Additionally, a much less expensive non-contact vibration sensor is used to make the demonstration more practical in its implementation.

This thesis will first describe the physics behind the main issue with creating a repeatable demonstration. A discussion of experiments conducted to optimize the demonstration will then be given. The optimal plate thickness, frequency bandwidth, and input voltage to the shakers are explored. Then the use of an eddy current sensor instead of a laser Doppler vibrometer is optimized. This thesis explores the use of a velocity sensor versus using a displacement sensor to create TR focusing of the plate's velocity or displacement. Finally, details are provided about how the demonstration was adapted for an exhibit at a wave propagation museum planned to be hosted at ETH University in Zurich, Switzerland.

2 Understanding the Time Reversal LEGO Demonstration

In traditional TR, a signal $s(t)$ is broadcast from a source into a system. A convolution of $s(t)$ with the impulse response of the system, $h(t)$, represents the response signal $r(t)$ that would be recorded at some receiver location in the system,

$$s(t) * h(t) = r(t). \tag{1}$$

If $s(t)$ is an impulsive signal, such as a delta function, $\delta(t)$, then $r(t) = h(t)$ and it can be used with further signal processing to achieve different types of TR focusing. Although this direct measurement of $h(t)$ seems theoretically easy to accomplish, it is difficult for realistic sources to produce a perfect impulse and attempts to do so result in a poor signal to noise ratio. Instead, the chirp method is used to indirectly obtain the impulse response.[31,32] In this method, a chirp, or sweep through a range of frequencies, is broadcast into the system as $s(t)$. The response to the chirp, $r(t)$, can then be cross correlated with the chirp to produce a band limited impulse response $h(t)$.

Once $h(t)$ is obtained, reversing it in time and broadcasting $h(-t)$ into the system yields

$$h(-t) * h(t) = y(t), \tag{2}$$

meaning that $y(t)$ is an autocorrelation result—a time-symmetric signal with a peak at the center—which corresponds to the peak focused amplitude that is characteristic of the time reversal process.[6] The method just described, simply broadcasting an unmodified $h(-t)$ is what we will

refer to as traditional TR. Two variants of TR which were mentioned in the introduction, clipping TR and deconvolution TR, will now be described.

The aim of the clipping TR method is to maximize the peak amplitude delivered to the focal location. The method is similar to traditional TR except that before the reversed and normalized impulse response is broadcast into the system, a clipping threshold C is defined between 0 and 1. Then, every data point in the normalized impulse response that has a value $> C$ is set equal to C and every data point that has a value $< -C$ is set equal to $-C$. The clipped signal is then normalized such that the clipped portions of the signal are at ± 1. The clipping of the signal alters the amplitude of the wave arrivals in the impulse response, but the timing of the waves is still preserved. Thus, the waves that are emitted in this clipped TRIR have a much larger relative amplitude than when using a traditional TRIR and the amplitude is increased at the focal location. Figure 1 shows a comparison between a traditional TRIR in Fig. 1(a) and a clipping TRIR in Fig. 1(b) along with their corresponding focal signals, Figs. 1(d) and 1(e), respectively. As seen in a comparison of the signals displayed in Figs. 1(d) and 1(e), the clipping TR method creates a higher peak amplitude focus but at the cost of a lower signal to noise ratio (the peak amplitude compared to the amplitudes elsewhere).

The experimental setup consists of a 1.27 mm thick aluminum plate which is elevated 2 cm above an optical table by 4 rubber stoppers placed at the corners of the plate. Custom LabVIEW software is used to create a logarithmic chirp signal with a bandwidth of 100-2000 Hz that lasts 0.5 s with 0.3 s of leading zeros and 0.2 s of trailing zeros. A 14-bit 4-channel Spectrum M2i.6022-exp generator card is used to output the chirp signal to one Mighty Dwarf 7W shaker. The acquisition is done with a PSV-400 SLDV and a 16-bit 4-channel Spectrum M2i.4931-exp digitizer card with a sampling frequency of 30 kHz. The SLDV is mounted above the plate and

aimed at a patch of retroreflective tape on top of the plate. The impulse response is measured, normalized, and reversed in time and then any additional signal processing techniques, such as clipping or deconvolution TR, are implemented. Finally, the resultant signal is broadcast from the shaker, creating a focus at the location where the SLDV measured the impulse response.
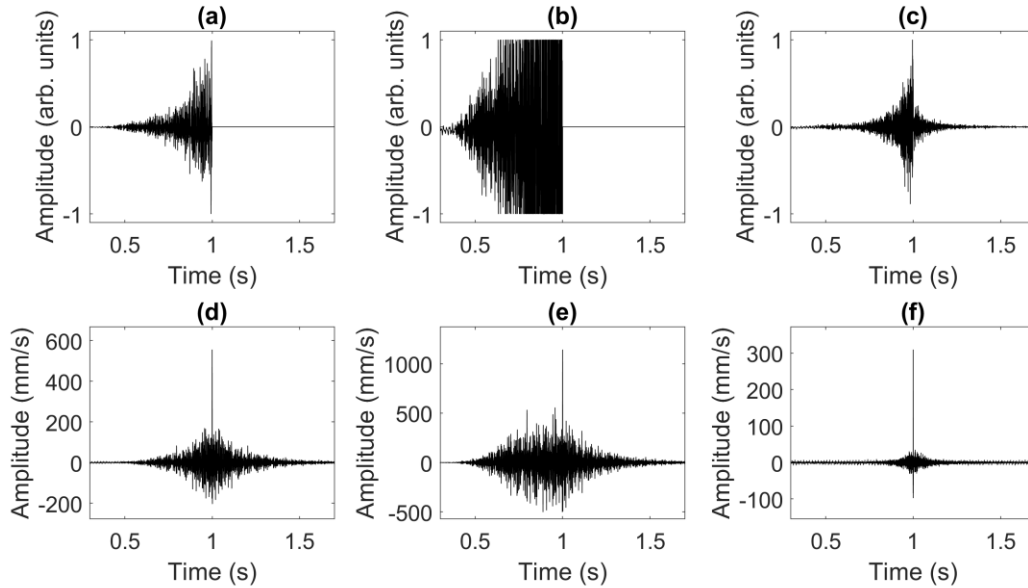
FIG. 1. (a) Traditional time reversed impulse response (TRIR) (b) Clipping TRIR. (c) Deconvolution TRIR. (d) Traditional time reversal (TR) focus. (e) Clipping TR focus. (f) Deconvolution TR focus.

The deconvolution or inverse filtering TR method seeks to maximize the signal to noise ratio of the focal signal by compensating for the resonances of the system. When the chirp signal described previously is broadcast into the system, its frequency content is affected by the resonances of the system transfer function, $H(f) = \mathcal{F}\{h(t)\}$, where $\mathcal{F}$ represents a Fourier transform operation. During traditional TR, with an impulsive signal, the focal signal is equivalent

to an autocorrelation of $h(t)$, or an autospectrum of $H(f)$. This means that system resonances impact the focal signal during the forward and backward steps of TR, hence why TR was originally called a matched signal process.[4,5] To compensate for these resonances, the inverse filter (or inverse transfer function) of the system $H^{-1}(f)$ is computed and then transformed into the time domain, normalized, time reversed, and broadcast into the system. When this modified impulse response is sent into the system, the inverse filter mixes with the resonances of the system, resulting in a relatively constant frequency response

$$H(f)^{-1} * H(f) = 1. \tag{3}$$

The inverse filter or deconvolution TRIR (Fig. 1(c)) results in a focal signal with a lower peak amplitude than traditional TR but yields a much better signal to noise ratio (Fig. 1(f)) than achieved with traditional TR or clipping TR.

The two methods described above, clipping TR and deconvolution TR, were in fact combined by Heaton *et al.* by first calculating the deconvolution TRIR, then applying the clipping TR method to that signal before broadcasting it. This was used to achieve a moderately clean focus signal but with a higher peak amplitude focus than results with deconvolution TR by itself. Despite having a high amplitude focus that could easily knock over a LEGO minifigure (see Fig. 2), an attempt to replicate the experiment using this method, using a somewhat lower input amplitude and a thinner plate, resulted in a repeatability of 45% in the success rate of knocking over the target LEGO minifigure when performed on an aluminum plate with 2 shakers for a set of 40 trials. 45% of the time the LEGO minifigure might be launched up to 4 cm into the air before falling down. The rest of the time the target LEGO minifigure would visibly vibrate (rattle on the plate surface) and rotate a bit, but it would not be launched into the air and instead would remain standing. The

thickness of the plate used in these experiments, 1.27 mm, was smaller than that of the plates used in Heaton's experiments, which contributed to a slightly higher repeatability than the approximate 30% repeatability Heaton *et al.* experienced. Optimization of plate thickness is discussed in Section 3.

(a)   **(b)**

FIG. 2. (color online) (a) Setup of the LEGO demonstration with two shakers in the background and the SLDV aimed at the minifigure in the middle. (b) The airborne minifigure after the focus.

In order to understand the reason for this low degree of repeatability, an SLDV was aimed at the top of a target LEGO minifigure's feet to measure the velocity over time of the minifigure during a broadcast of the TRIR. Then the experiment was repeated with the SLDV aimed to measure the velocity of the plate below its feet. The velocity of the minifigure's feet (Fig. 3(c)) had several abrupt increases in velocity, each followed by a consistent downward sloping velocity, whose slope corresponds to the acceleration due to gravity. Thus, it was discovered that the minifigure was repeatedly losing contact with the top of the plate for just a few milliseconds at a time, but with enough vertical displacement from the plate to often miss the main focal event entirely. This discovery led to the critical understanding that if the smaller vibrations leading up

9

to the focal event (termed side lobes in the TR literature) were high enough in amplitude, they would cause the minifigure to lose contact with the plate and thus decrease the chances of the minifigure being knocked over by the main focal event.
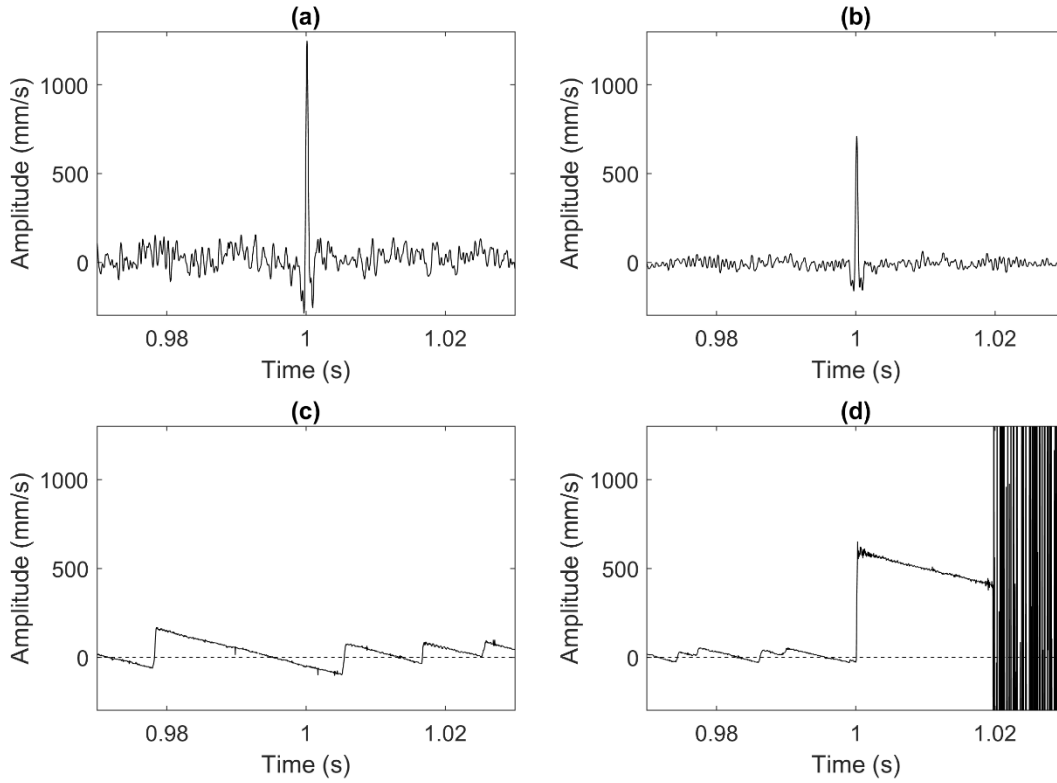
FIG. 3. (a) Plate velocity during deconvolution plus clipping time reversal (TR) focusing. (b) Plate velocity during deconvolution TR focusing. (c) LEGO minifigure velocity measured at their feet during deconvolution plus clipping TR. (d) LEGO minifigure velocity measured at their feet during deconvolution TR.

With this understanding in mind, it is clear that a better approach to increasing the repeatability of the demonstration is to use the cleanest TR method possible, such as only

deconvolution TR without any clipping to minimize the amplitude of the side lobes while maintaining enough amplitude in the focus to launch the minifigure. The repeatability experiment was performed again, this time only using deconvolution TR, and the resulting repeatability was 75% for a set of 40 trials. Figure 3 shows a comparison between clipping TR and deconvolution TR focal signals and examples of how LEGO minifigures react to those signals. Optimization of this approach is discussed in the next section.

3 Optimizing the Demonstration in a Laboratory

A set of experiments were designed and performed to optimize parameters of the demonstration for increased repeatability. These included plate thickness, chirp frequency range, and TRIR amplitude. While Heaton *et al.*[28] explored the use of different types of plate materials to use for the demonstration, the thickness of the plate was not previously explored. TR experiments were performed on three different aluminum plates whose thicknesses were 6.35 mm, 3.18 mm, and 1.27 mm. The dimensions of the 6.35 mm and the 3.18 mm thick plates were 0.91 m by 1.22 m, whereas the 1.27 mm thick plate had been cut and bent into the shape of a bridge, which is explained more later, before performing the following experiments. Plate thickness is expected to play a more significant role in the trends observed than the plate's shape or area. Four shakers were used with their amplification settings at maximum on each plate along with a chirp bandwidth of 100-2000 Hz. The shakers were placed near the corners of the plate, but shaker

position was not explored in detail. Two metrics were used to quantify results: temporal quality and peak amplitude. For these experiments, temporal quality is defined[28,33] as

$$\xi_T = \sqrt{\frac{[A_P]^2}{\frac{1}{M}\sum_{m=1}^{M}[A(x_0,y_0,z_0,m)]^2}} \,, \tag{4}$$

where A_P is the peak amplitude at the focus location, $A(x_0, y_0, z_0, m)$ is an amplitude measurement at the focal location, (x_0, y_0, z_0) at a given time sample m, and M is the total number of time samples in the signal. As plate thickness decreased, several trends were noticed. As indicated in Table I, smaller plate thickness yields both a higher peak amplitude as well as a higher temporal quality, which are both desirable traits for time reversal focusing.

TABLE I. Results when using time reversal in different thickness aluminum plates for peak amplitude of the time reversal focusing, A_P, and temporal quality, ξ_T.

Thickness (mm)	A_P (mm/s)	ξ_T
6.35	96	60.2
3.18	662	69.4
1.27	1490	73.9

Another noticeable trend was that when the demonstration utilizes a thicker plate, the sound radiated by the plate is louder and has a shrill sound quality, which is undesirable for a museum demonstration. The bending waves (or the zeroth-order, antisymmetric Lamb waves) in the plate, which are assumed to dominate in these experiments, are dispersive. The phase speed

of these bending waves, c_b, is proportional to the square root of frequency, f (and angular frequency, $\omega = 2\pi f$) and proportional to the square root of the plate thickness, h,

$$c_b = \left(\frac{\omega^2 E h^2}{12\rho(1-v^2)}\right)^{\frac{1}{4}},\qquad(5)$$

where E is the Young's modulus, ρ is the mass density, and v is Poisson's ratio.[34] Figure 4 plots the expected wave speeds for the three plates studied over the frequency range of interest. As the bending wave speed increases, the radiation efficiency of sound generated by these waves traveling in the plate generally increases (for subsonic wave speeds).[34] This is the reason why thicker plates and higher frequencies are heard better and result in a shrill sound quality because of the higher bending wave speeds. Thus, thinner plates more desirable for the museum demonstration because the noise made by the demonstration can be annoying for users and others nearby. However, if the plate is too thin then it is not structurally stable enough to support the weight of the equipment for the demonstration. From these experiments, it was concluded that the 1.27 mm thick plate was optimal.

Next, the interaction between the plate and the target LEGO minifigure was optimized. When the downward acceleration of the plate underneath the minifigure exceeds the acceleration due to gravity, the minifigure loses contact with the plate. Thus, if the downward acceleration exceeds 9.8 m/s^2 just prior to the TR focusing peak then the minifigure is not maximally launched into the air, leading to the repeatability problem described in Section 2. Thus, reducing the acceleration of the plate prior to the arrival of the focusing peak increases the amount of time that the minifigure is in contact with the plate and the likelihood that the minifigure will be hit by the main focal peak and be launched off of the plate. Acceleration amplitude, $a(t)$, in time-harmonic motion is a function of velocity amplitude $v(t)$ and angular frequency ω,

$$a(t) = \omega\, v(t). \tag{6}$$

A parametric study was conducted on amplitude and frequency bandwidth to find optimal values for both of these parameters. Optimal values of amplitude and frequency bandwidth are defined as the values that lead to the target minifigure being knocked over most repeatably while leaving the other non-target minifigures on the plate standing. There are trade-offs, however, with both amplitude and frequency. Lower amplitudes and lower frequencies both decrease the acceleration of the plate, but the amplitude still needs to be high enough to launch the target minifigure during the main focal event, and high frequencies are desirable because they increase the spatial confinement of the TR focusing, reducing the likelihood of nearby minifigures being knocked over.
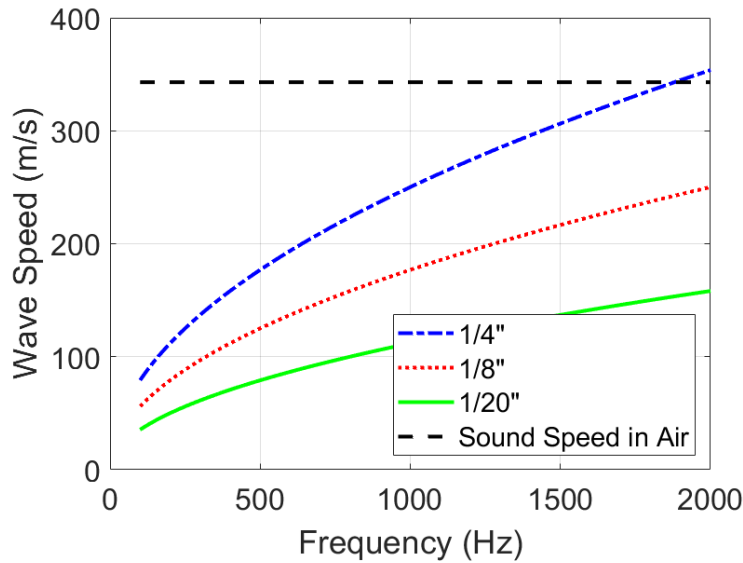

FIG. 4. (color online) Bending wave phase speed as a function of frequency for aluminum plates of different thicknesses.

First, repeatability as a function of the frequency bandwidth of the chirp signal was studied. Repeatability experiments were conducted on a set of fixed frequency bandwidths as well as varying frequency bandwidths. These experiments were carried out on a 0.91 m by 1.22 m by 1.27 mm aluminum plate with 4 shakers and an SLDV. In the fixed bandwidth experiments, the chirp signal used to get the impulse response was set to a fixed bandwidth of 1000 Hz. A set of 40 trials were performed for each of 12 different frequency bandwidths with starting frequencies ranging from 100 Hz to 1200 Hz in 100 Hz intervals (Fig. 5(a) gives the starting and ending frequencies for all of the bandwidths tested). In an individual trial, the forward and backward steps of TR were conducted and then a LEGO minifigure was placed at the focal location to see if it would be knocked over. Nine additional minifigures were placed at other locations on the plate at least 10 cm away from the shakers and from the focal location. A successful trial was one in which the target minifigure was knocked over (fell down). The results of these fixed-bandwidth experiments are shown as percentages of success (repeatability) in Fig. 5(a), with 100% meaning that the target minifigure was knocked over 40 out of 40 times. Note that the results in Fig. 5(a) represent $12 \times 40 = 480$ individual trials of the demonstration. The results indicate that the 1000 Hz bandwidths at lower frequencies were more effective in launching the target minifigure, and the success rate (or repeatability) dropped off quickly as frequency increased.
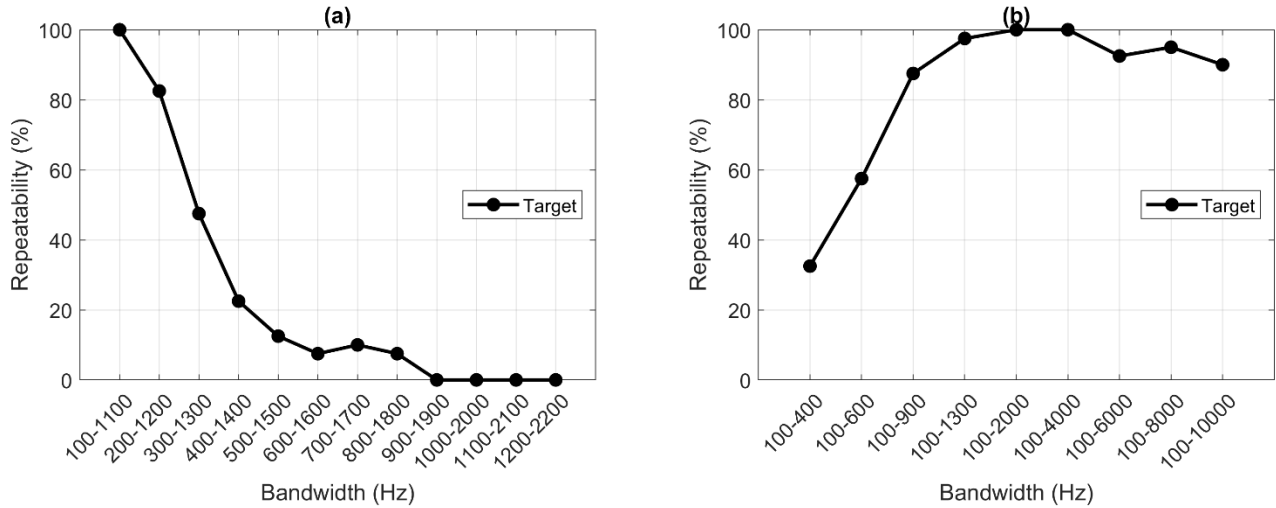
15

FIG. 5. Repeatability tests of the demonstration. Each data point represents the success rate (repeatability percentage) from 40 trials to knock over the target minifigure. (a) Repeatability when using various fixed frequency bandwidths of 1000 Hz. (b) Repeatability when varying the bandwidth.

To explore the effects of varying the bandwidth with a fixed starting frequency, 40-trial repeatability experiments were performed for 9 different bandwidths all starting at 100 Hz but ending at frequencies ranging from 400 Hz to 10 kHz. Figure 5(a) shows that chirps centered at lower frequencies are better, but Fig. 5(b) shows that the inclusion of some higher frequency content increases the repeatability.

Next, a similar set of repeatability experiments were conducted for different TRIR broadcast amplitudes to understand the effect of amplitude on the repeatability of the demonstration. At this point, the plate had been cut and bent into the shape of a bridge because the museum demonstration would utilize a bridge-shaped plate (one potential application of TR that visitors could understand is to detect and locate cracks in bridges and other structures). The

16

TR experiments were performed starting with a low amplitude TRIR that rarely knocked over the target minifigure and was not strong enough to ever knock any of the other minifigures over. 40 trials were performed for each of 12 different input amplitudes. These repeatability results are shown in Fig. 6. The SLDV was again used along with a frequency bandwidth of 100-2000 Hz.
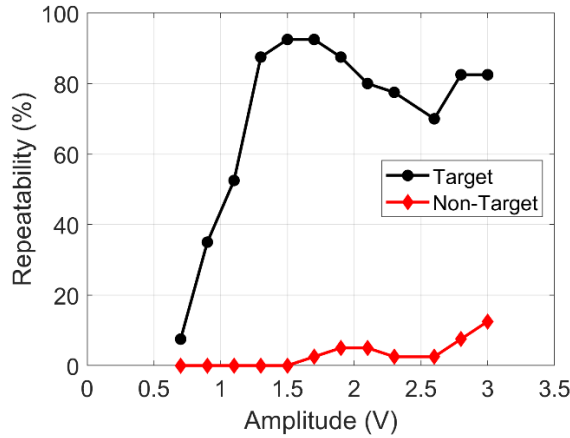

FIG. 6. (color online) Repeatability of the demonstration when using different input amplitudes to the shaker sources. Here the percentage of the times that the target minifigure was knocked over is tracked as well as the percentage of the times that non-target minifigures fell down. Each data point in the figure represents the success rate (repeatability percentage) for 40 trials conducted at each input amplitude. The scanning laser Doppler vibrometer was used here to create velocity foci for these experiments.

Although the specific input voltages greatly depend on the instrumentation used, the experimental results in Fig. 6 illustrate that a certain amplitude threshold is needed to repeatedly knock over the target minifigure. However, too much amplitude actually reduces the likelihood that the target will be knocked over, as well as increasing the likelihood of knocking over other

minifigures. Both the reduction of knocking over the target and the increase in knocking over non-target minifigures can be explained by the higher amplitude side-lobes caused by a higher output amplitude from the shakers. Higher amplitude side lobes can cause the target minifigure to be in the air when the main focal event happens and the higher side lobes will correspond to larger vibrations elsewhere in the plate, knocking over the non-target minifigures. It is important to note that because the museum exhibit will only use 2 shakers, these repeatability vs amplitude experiments were done with 2 shakers whereas the repeatability vs frequency experiments were done using 4. This is the main reason why the highest repeatability achieved in these experiments was 92.5% (37/40) despite being performed with a bandwidth of 100-2000 Hz which achieved 100% repeatability in the previous experiments (see Fig. 5 (b)).

Based on the optimization experiments for the plate thickness, input amplitude, fixed bandwidth, and varying bandwidth, the optimal parameters for this specific setup with two shakers were determined to be 1.27 mm plate thickness, 1.5 V input amplitude to the shakers, and 100-2000 Hz frequency range for the chirp signal. With these optimal parameters, a repeatability of 92.5% was achieved. When using four shakers instead of two and an input voltage of 1 V, 100% repeatability was achieved for a set of 80 trials.

4 Eddy Current Sensor

The SLDV was used for all of the laboratory experiments previously discussed, but it is too expensive to use in a practical demonstration setting, such as the planned museum exhibit. One relatively inexpensive sensor that was still able to measure the 100-2000 Hz frequency range

adequately was an eddy current sensor (ECS), which is a non-contact displacement sensor. The ECS uses an active coil of wire to generate an alternating magnetic field in the vicinity of a conducting surface. The magnetic field causes small electric currents called eddy currents to be induced in the conductive surface, in this case an aluminum plate. These eddy currents oppose the excitation current and cause a drop in voltage across the sensor which is measured and converted to an output voltage that is proportional to the displacement between the plate and the sensor head. An additional advantage of the ECS over the SLDV is its portability, which is useful for performing this demonstration in various venues with ease. The purpose of this section is to contrast the use of the ECS (approximate cost \$1.3k USD), a displacement sensor, to that of the SLDV (approximate cost \$250k USD), a velocity sensor, in TR experiments.

The ECS sensor used here is a Micro-Epsilon DT3001-U8-A-SA eddy current measuring system with a sensing range of 8 mm from the ECS surface. Because the ECS outputs a voltage proportional to displacement relative to the sensing head, the signal response has a DC offset (Fig. 7(a)) corresponding to the overall distance between the plate and the ECS. The DC offset was removed by subtracting the mean of the dynamic signal recordings, as in the chirp response pictured in Fig. 7(b). The ECS measurement range corresponds to an output voltage range from .5 V to 9.5 V. To allow for motion of the plate toward and away from equilibrium, it is optimal to place the plate well within the measuring range so that the AC voltages won't exceed the dynamic range of the digitizer card. This ECS also picks up quite a bit of low frequency noise so a second-order Butterworth filter that had a bandpass response between 100 and 2000 Hz was used to filter the signal response, as shown in Fig. 7(c). After removing the DC offset and filtering the chirp response signal the cross correlation is performed to obtain the impulse response.
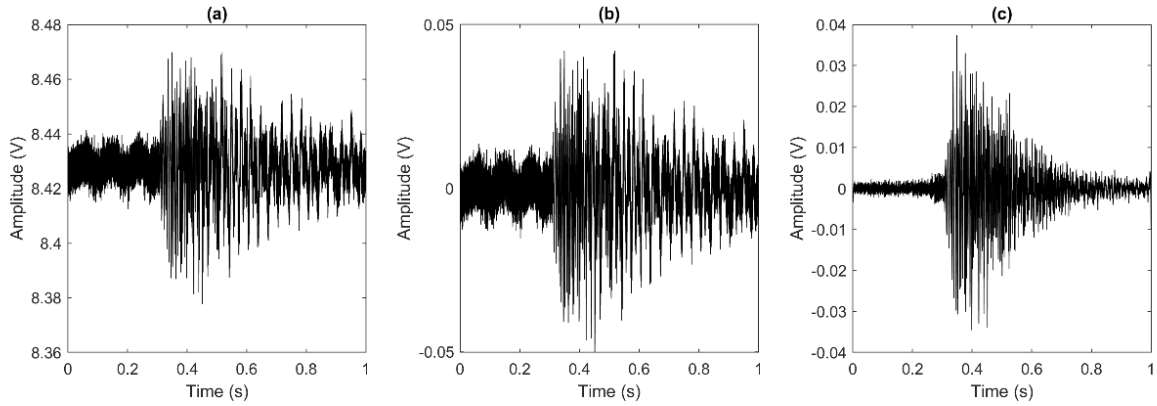
FIG. 7. Example signals recorded with the eddy current sensor. (a) Unfiltered chirp response with DC offset. (b) Unfiltered chirp response with DC offset removed. (c) Filtered chirp response with DC offset removed.

Because the ECS is a displacement sensor, the impulse response obtained between the shaker and the ECS is a displacement signal. Thus, the use of this impulse response results in a TR focus that has a displacement peak (Fig. 8(a)). If this displacement focus is recorded using a velocity sensor, such as an SLDV, the signal would instead show up as the "N-shaped" derivative of the displacement focus signal (Fig. 8(b)). If an SLDV is used to obtain the impulse response, which is subsequently used to create a TR focus, a SLDV recording will show a standard symmetric TR focus that has a velocity peak (Fig. 8(d)). A displacement recording of that velocity TR focus will appear as a backwards "N-shaped" integral of that focus signal (Fig. 8(c)).
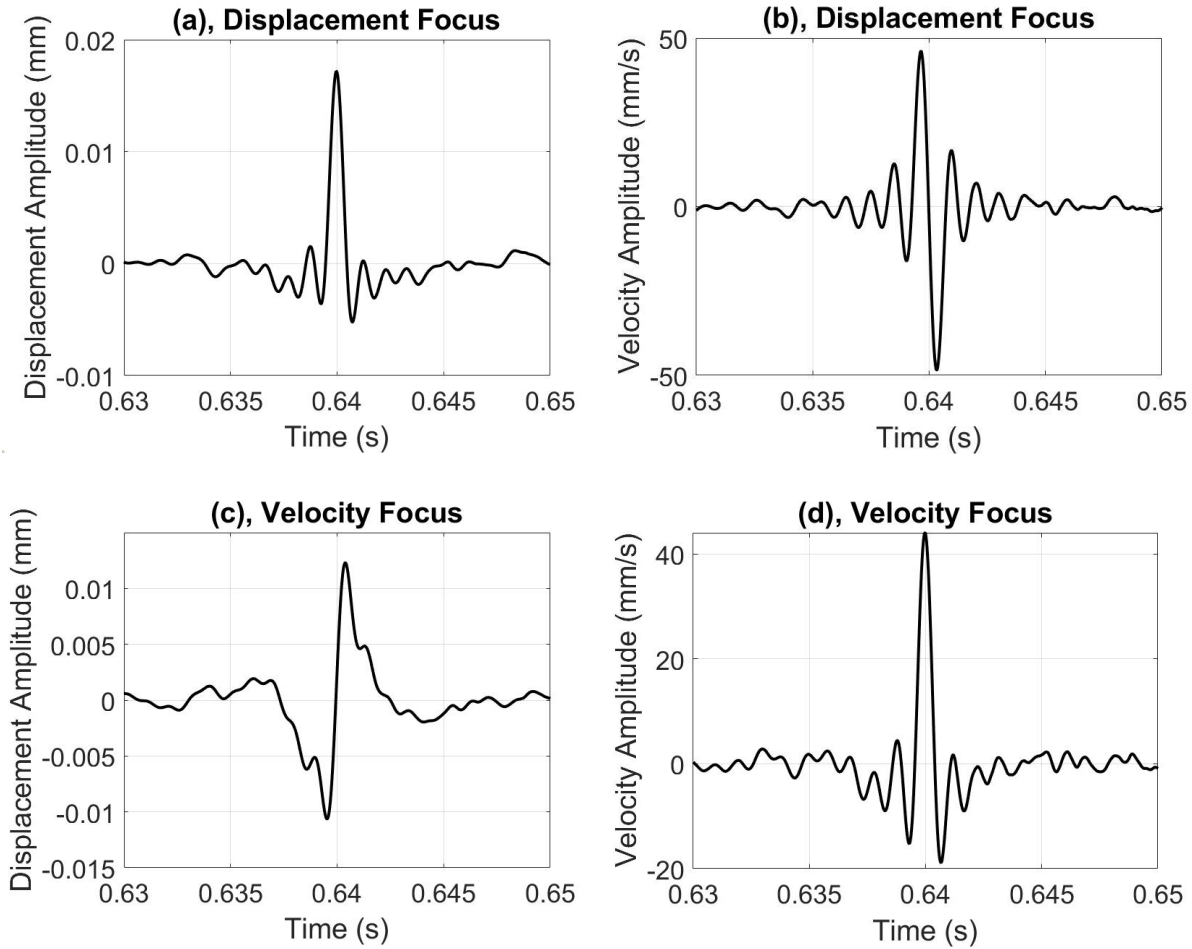
FIG. 8. (a) Displacement amplitude recording during displacement time reversal (TR) focusing. (b) Velocity amplitude recording during displacement TR focusing. (c) Displacement amplitude recording during velocity TR focusing. (d) Velocity amplitude recording during velocity TR focusing.

It is conceivable that the ESC could be used to create a backwards "N-shaped" displacement focus signal, similar to the one in Fig. 8(c), by modifying the displacement impulse response. This would allow a peak velocity to be created during the focusing. One way to create a backwards "N-shaped" focus and mimic the phase shift that an integral imposes would be to

introduce a phase shift of -90° at all frequencies in the TRIR. The displacement during this TR

focusing would look similar to that pictured in Fig. 8(c) but the velocity would look like that

pictured in Fig. 8(d). A velocity sensor could be used, with a modified impulse response, to

create a focusing like that pictured in Fig. 8(b) to create a displacement peak in the focusing like

that pictured in Fig. 8(a). Applying a 90° phase shift to the velocity TRIR would create a velocity

signal like that shown in Fig. 8(b) during TR focusing, while the displacement signal would look

like that shown in Fig. 8(a). An accelerometer, or another acceleration-based vibration sensor,

may also be used to create a displacement or a velocity TR focus peak by applying a 180° or 90°

phase shift to the TRIR, respectively. The authors verified that each of these experiments work

as described by using the ECS and SLDV. A similar idea called phase inversion or pulse

inversion introduced the idea of applying a 180° phase shift to the TRIR to create a symmetric,

negative-value, TR focus peak[35]. Third order phase symmetry analysis introduced the idea of

implementing 120° and 240° phase shifts to the TRIR so that 0°, 120°, and 240° phase shifted

TRIR signals could be used to create 3 different focal signals that may be combined in such a

way to detect the presence of even or odd harmonics caused by nonlinearities in a high amplitude

time reversal focus.[36]

     With the ability to create different shaped focal signals comes the question of what focal

shape will launch a LEGO minifigure into the air the highest to increase the chances of knocking

over the minifigure? In Section 3 it was found that lower velocity and acceleration amplitudes

were desirable to reduce the likelihood of the LEGO minifigure losing contact with the plate and

being in the air when the focus peak arrives. The optimal, local motion of the plate would be a

large upward velocity, to give the minifigure a large upward momentum, followed by a large

downward acceleration (steep negative slope of velocity versus time) such that the minifigure

would lose contact with the plate and the plate would travel downward while the minifigure continued to rise further above the plate. The higher the minifigure travels, the more likely it will be to fall over upon returning to the plate surface.

Because both the displacement focus and the velocity focus, measured in velocity (Fig. 8(b) and Fig. 8(d), respectively), exhibit a large, positive-velocity peak followed by a large negative slope, it is expected that both types of foci could launch a LEGO minifigure. Experiments confirmed that a displacement focus and a velocity focus were equally capable of launching the LEGO minifigure and knocking it over. A set of 40-trial repeatability tests, with results shown in Fig. 9, revealed that the ECS provided a similar overall repeatability trend as the experiments done with the SLDV in Section 3 (compare Fig. 9 to Fig. 6). These repeatability trials were also performed with only 2 shakers on the bridge-shaped plate as was done with the SLDV repeatability versus amplitude trials. Using the ECS and 2 shakers on the bridge, the demonstration had a repeatability up to 92.5% (37/40) at an input voltage of 1.8 V to the shakers, which is the same maximum repeatability achieved with the SLDV and 2 shakers on the bridge.
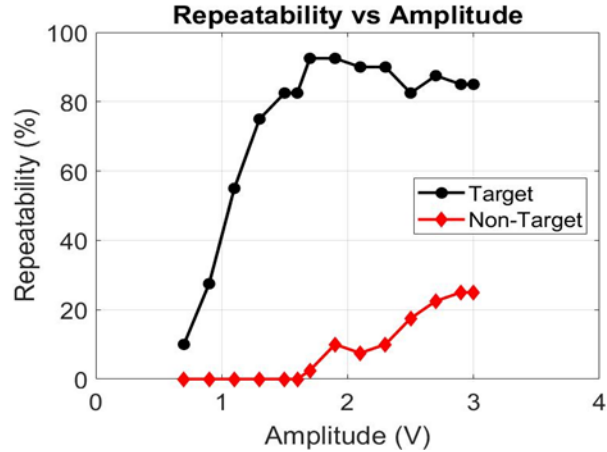
FIG. 9. (color online) Repeatability of the demonstration when using different input amplitudes to the shaker sources. Here the percentage of the times that the target minifigure was knocked over is tracked as well as the percentage of the times that non-target minifigures fell down. Each data point in the figure represents the success rate (repeatability percentage) for 40 trials conducted at each input amplitude. The eddy current sensor was used here to create displacement foci for these experiments.

While low frequencies were found to contribute significantly to the successful launching of the target minifigure, they also have larger wavelengths and lead to a wider spatial focus. This is not desirable because a larger focal area will be more likely to knock over non-target minifigures. Because the ECS is more sensitive to lower frequency motion than the SLDV, the spatial extent of the focusing was a concern. Also, since the ECS induces currents in the target material, the manufacturer states that the required sensing area is about 3-5 cm in diameter, much larger than the sensing area of the SLDV (~30 μm). This larger sensing area of the ECS also likely contributes to a wider focus. Heaton *et al.*[28] showed what the velocity profile of a velocity focus looks like. For comparison, in Fig. 10 the displacement profile of a displacement focus at the time of maximal

focusing using the ECS is shown. Note that the scan area was 51 by 51 cm, and the flat, top surface of the bridge-shaped plate was 61 by 91 cm in area. The full width half maximum of this displacement focus was determined to be 6.2 cm.
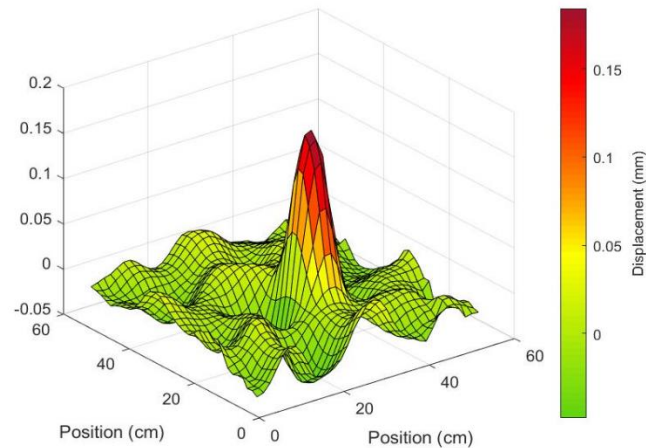

FIG. 10. (color online) Surface plot of a displacement time reversal focus peak during the time of peak focusing. An eddy current sensor was used to obtain the impulse response and a scanning laser Doppler vibrometer was used to record the displacement at each scan position.

5 Museum Exhibit

This section will focus on describing efforts to make the demonstration more practical for the museum exhibit at focusTerra, the Earth & Science Discovery Center of ETH Zurich, Switzerland. For the museum exhibit setup, a bridge-shaped plate that was 1.5 mm thick, with a top surface measuring 91 cm by 61 cm, was used with two Mighty Dwarf 7W shakers. The shakers

were placed on opposite corners of the bridge. The ECS was mounted on three computer-controlled, FUYU FSL40 linear motion stages in the shape of an "H" so that the ECS could be translated in two dimensions underneath the plate and take displacement recordings. The data acquisition and generation were managed with a NI USB-6211 multifunction input/output device. A touch screen user interface along with an overhead camera allows users to select a location on the plate where they want to create a TR focus. The translation stages underneath the plate then move the ECS to the selected location and a chirp is emitted from each shaker while the ECS records the response between each shaker and the target location. The impulse responses are determined through filtering and cross correlation. Then, the ECS is moved away from the target location and the two shakers simultaneously broadcast their respective TRIRs, creating a focus at the target location. The setup is shown in Fig. 11.

The bridge can be populated with LEGO minifigures, arranged to resemble two opposing soccer teams. Visitors to the museum exhibit then take turns trying to knock over the players of the other team using the TR focusing. The user interface provides further information on how TR works to focus waves to a selected location, its application in science and industry, as well as animations of the focusing acquired with an SLDV system. Some variables that made the demonstration more practical and suitable for a museum exhibit contributed to a reduced repeatability compared to the repeatability of the laboratory demonstration at Brigham Young University described previously. These include the user's accuracy when interacting with the touch screen, camera alignment precision, and hardware limitations. If the user does not touch the screen exactly where the target minifigure is or the positioning system for the ECS is not aligned with the camera view on the touch screen, the target minifigure might not be standing at the exact TR focal spot. The low output impedance of the NI USB-6211 required an impedance
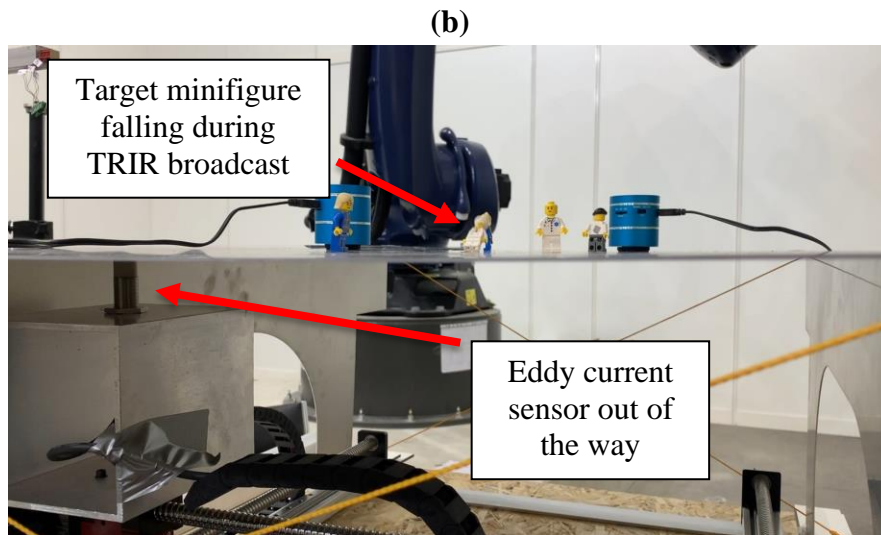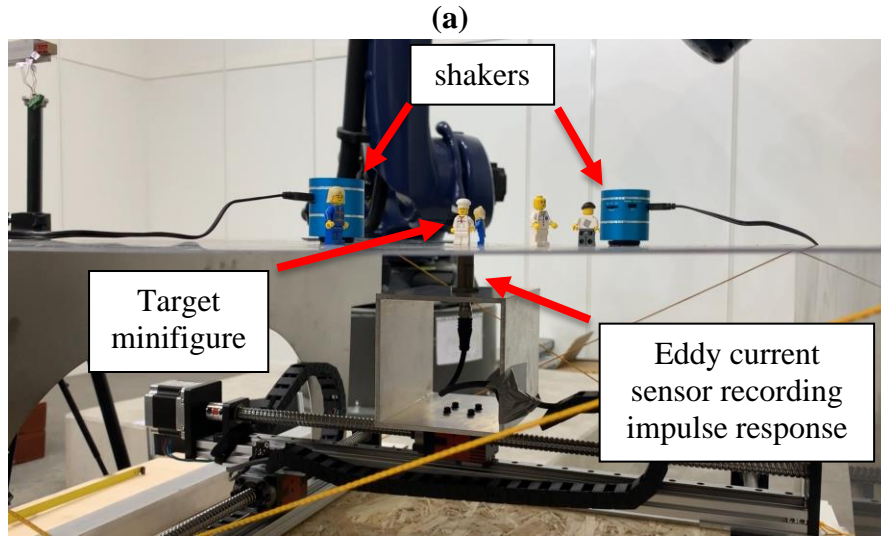
26

FIG. 11. (color online) Photograph of the setup for the focusTerra exhibition hall. (a) The eddy current sensor recording the impulse response at the location of the target minifigure (b) The target minifigure falling during the broadcast of the time reversed impulse response (TRIR).

matching stage to properly condition the signals sent to the mighty dwarf speakers. This was done using LF147J operational amplifiers from Texas Instruments. To power the LF147J, a DPBW06F-12 DC-DC converter from Mean-Well was used. The switching from this converter created a high frequency noise on the acquired signals; however, it did not seem to affect the signals in the frequency band of interest. Also, in an effort to streamline the processing of data, the experiment was tested without bandpass filtering the recordings. These factors led to a decrease in repeatability. The repeatability was tested with a 100-2000 Hz chirp, no averaging (the chirp signals were played once per shaker), and the forward and backward input voltages to the shakers set to 0.3 V and 1.6 V, respectively, with the volumes on both shakers manually turned all the way up. Out of 90 trials, the target minifigure visibly jumped in the air 93% of the time but only fell over 63% of the time, and non-target minifigures were knocked over 0% of the time. However, because the demonstration is presented in a game format, a decreased repeatability is desirable because it adds an element of unpredictability, which makes it more fun for users.

One issue with the museum setup, specifically the bridge shape of the aluminum plate, was that the top surface of the bridge bowed by a few millimeters in the center compared to the edge. Since the ECS only had a displacement measurement range of 8 mm, the standoff distance between the ECS and the underneath side of the bridge's top surface needed to be monitored. Further, the bridge was only 1.5 mm thick and so it was prone to swaying when users interacted with it. To reduce the swaying, strings were attached from the upper corners of the bridge to the opposite sides of the base, creating a cross on each end. For the museum setup, the feet of the bridge will also be fixed in place. Stiffness of the plate and different boundary conditions may also have been factors that affected repeatability.

An issue currently being addressed is the radiated noise of the demonstration being heard by others in the museum. Figure 12 shows the exhibition space (on the floor) is surrounded by offices and studying facilities for students, making the need for noise reduction apparent. The findings introduced in this paper have allowed the demonstration to be much quieter than the previous version of the demonstration presented by Heaton et al.[28] The use of a thinner plate and a reduced bandwidth both help to reduce the radiated noise. The deconvolution TR technique and the use of multiple shakers allows smaller vibration amplitudes to be used while still yielding a sufficiently large focal amplitude to launch the minifigure.

FIG. 12. (color online) Photograph of the focusTerra exhibition hall where the demonstration will be set up.

The easiest way to reduce the radiated noise levels is to decrease the upper bound of the frequency range of the chirp and the amplitude of the signal. This reduces the amount of high

frequency noise radiated by the experiment which can make it less disturbing. However, reducing the bandwidth of the chirp will also cause the focus to be less spatially confined and the demonstration may not work as well because non-target minifigures will be more likely to get knocked over. Currently a bandwidth of 20-1200 Hz is being considered. This will decrease the amount of high frequency content, which human ears are particularly sensitive to. The frequencies from 1200-2000 Hz would also have higher radiation efficiencies than the frequencies from 20-1200 Hz. However, this reduced bandwidth should also decrease the repeatability of the demonstration by a small amount from 63%. Fortunately, this is tolerable since a decreased repeatability provides a game of chance and the decrease in repeatability in the laboratory experiments due to a bandwidth change from 100-2000 Hz down to 100-1300 Hz only reduced the repeatability by 2.5% (see Fig. 5(b)). The frequencies from 20-100 Hz are not expected to change this result since the shakers don't emit those frequencies well.

The translation stages that moved the ECS underneath the plate emitted some high frequency noise during motion. Slowing down the ECS positioning system motion underneath the plate proved effective in reducing the amount of high frequency noise made. It also helped to reduce induced swaying of the bridge caused by the starting and stopping of the positioning system. Another possibility being considered to reduce the radiated noise of the demonstration is to place a clear Plexiglas enclosure around the demonstration to contain the noise. Furthermore, sound absorbing material is placed below the plate and on two additional faces of the enclosure. The front wall includes an opening such that users can place the LEGO minifigures on the bridge.

6 Conclusion

This paper proves a better physical understanding and optimization of a demonstration of Time Reversal (TR) acoustics introduced by Heaton *et al.*[28] First, a comparison between traditional TR, deconvolution TR, and clipping TR was presented. This led to the experimental discovery that large amplitude side-lobes were causing the target minifigure to bounce prematurely, sometimes causing it to be in the air during the main focal event and not be knocked over. This critical insight indicates that the best TR method to use for the demonstration is deconvolution because the deconvolution method leads to a better signal to noise ratio than is typical of traditional TR or clipping TR and therefore smaller side-lobes.

Several parameters of the setup and the TR process were optimized including the thickness of the plate, frequency range of the chirp, and the amplitude of the time reversed impulse response (TRIR). Three different plate thicknesses were studied, and it was found that thinner plates yield higher peak amplitudes as well as a higher temporal quality. These are both desirable traits for a TR focal signal, so long as the structure is strong enough to stand and support any required equipment. Additionally, less noise is radiated from thinner plates because the waves are more likely to be traveling at subsonic speeds.

For chirp frequency range optimizations, one set of repeatability experiments was performed while varying the upper bound of the chirp and holding the lower bound constant, and another set of experiments were performed while holding the bandwidth constant and raising the lower and upper bounds of the chirp together. It was found that lower frequencies are most effective in knocking over the target minifigure but that higher frequencies are also necessary to

reduce the number of times non-target minifigures were knocked over by reducing the spatial extent of the focusing. In the end, the frequency range of 100-2000 Hz was determined to be optimal for the demonstration.

Another set of repeatability experiments was performed while varying output amplitude of the TRIR. An important tradeoff discovered was that there needs to be enough amplitude to knock over the target but that too much amplitude would cause the side-lobes to be too large and the minifigure could prematurely bounce into the air and miss the main focal event. Therefore, a balance must be found, but the specific amplitude will vary from setup to setup. The optimal parameters for our specific setup with two shakers were determined to be 1.27 mm plate thickness, 1.5 V input amplitude to the shakers, and 100-2000 Hz frequency range for the chirp signal. With these optimal parameters, a 92.5% repeatability for a set of 40 trials was achieved. Additionally, when using four shakers instead of two and an input voltage of 1 V, a 100% repeatability for a set of 80 trials was achieved.

The main differences in the state of the demonstration before and after the contributions of this paper are that the launch height of the minifigure is lower, but it is quieter and much more repeatable, a cheaper sensor was implemented, and there are less non-target minifigures falling over. These optimizations made the demonstration suitable for implementation as an exhibit in a wave propagation museum at ETH Zurich in Switzerland. Due to hardware limitations, the repeatability in the museum exhibit was 63%, which was lower than the repeatability found in the laboratory. Fortunately, the lower repeatability provides for a more fun game of chance and the demonstration remains an effective way to visualize the focusing power of TR acoustics.

Bibliography

[1] M. Fink, "Time reversed acoustics," Phys. Today **50**, 34-40 (1997).

[2] B. E. Anderson, M. Griffa, C. Larmat, T. J. Ulrich, and P. A. Johnson, "Time reversal," Acoust. Today **4**(1), 5–16 (2008).

[3] B. E. Anderson, M. C. Remillieux, P.-Y. Le Bas, and T. J. Ulrich, "Time reversal techniques," in Nonlinear Acoustic Techniques for Nondestructive Evaluation, 1st ed., edited by T. Kundu, (Springer and Acoustical Society of America, New York, 2018), Chap. 14, pp. 547–581.

[4] A. Parvulescu and C. S. Clay, "Reproducibility of signal transmission in the ocean," Radio Elec. Eng. **29**, 233–228 (1965).

[5] C. S. Clay and B. E. Anderson, "Matched signals: the beginnings of time reversal," Proc. Meet. Acoust. **12**, 055001 (2011).

[6] M. Tanter, J.-L. Thomas, and M. Fink, "Time reversal and the inverse filter," J. Acoust. Soc. Am. **108**(1), 223-234 (2000).

[7] M. Tanter, J. F. Aubry, J. Gerber, J.-L. Thomas, and M. Fink, "Optimal focusing by spatiotemporal filter. I. basic principles," J. Acoust. Soc. Am. **110**, 37-47 (2001).

[8] T. Gallot, S. Catheline, P. Roux, and M. Campillo, "A passive inverse filter for Green's function retrieval," J. Acoust. Soc. Am. **131**, EL21-EL27 (2011).

[9] B. E. Anderson, J. Douma, T. J. Ulrich, and R. Snieder, "Improving spatio-temporal focusing and source reconstruction through deconvolution," Wave Mot. **52**, 151-159 (2015).

[10] M. Fink, "Time-reversal acoustics in biomedical engineering," Annual Rev. Biomed. Eng. **5**(1), 465-497 (2003).

[11] M. Fink, "Time reversal and phase conjugation with acoustic waves: industrial and medical applications," Lasers and Electro-Optics **3**, 2334-2335 (2005).

[12] G. F. Edelmann, H. C. Song, S. Kim, W. S. Hodgkiss, W.A. Kuperman, and T. Akal, "Underwater acoustic communications using time reversal," IEEE Journal of Oceanic Engineering **30**(4), 852-864 (2005).

[13] G. Zhang, J.M. Hovem, D. Hefeng, and L. Liu, "Coherent underwater communication using passive time reversal over multipath channels," Appl. Acoust. **72**(7), 412-419 (2011).

[14] C. He, Q. Zhang, and J. Huang, "Passive time reversal communication with cyclic shift keying over underwater acoustic channels," Appl. Acoust. **96**(9) 132-138 (2015).

[15] B. E. Anderson, T. J. Ulrich, P.-Y. Le Bas, and J. A. Ten Cate, "Three dimensional time reversal communications in elastic media," J. Acoust. Soc. Am. **139**(2), EL25-EL30 (2016).

[16] C. Larmat, J.-P. Montagner, M. Fink, Y. Capdeville, A. Tourin, and E. Clevede, "Time-reversal imaging of seismic sources and applications to the great Sumatra earthquake," Geophys. Res. Lett. **33**(19), L19312 (2006).

[17] C. Larmat, J. Tromp, Q. Liu, and J.-P. Montagner, "Time-Reversal location of glacial earthquakes," J. Geophys. Res. **113**(B9), B09314 (2008).

[18] C. Larmat, R. A. Guyer, and P. A. Johnson, "Tremor source location using time-reversal: selecting the appropriate imaging field," Geophys. Res. Lett. **36**(22), L22304 (2009).

[19] C. S. Larmat, R. A. Guyer, and P. A. Johnson, "Time-reversal methods in geophysics," Phys. Today **63**(8), 31-35 (2010).

[20] I. Rakotoarisoa, J. Fischer, V. Valeau, D. Marx, C. Prax, and L.-E. Brizzi, "Time-domain delay-and-sum beamforming for time-reversal detection of intermittent acoustic sources in flows," J. Acoust. Soc. Am. **136**(5), 2675–2686 (2014).

[21] A. Mimani, Z. Prime, C. J. Doolan, and P. R. Medwell, "A sponge-layer damping technique for aeroacoustic time-reversal," J. Sound Vib. **342**, 124-151 (2015).

[22] A. Mimani, Z. Prime, D. J. Moreau, and C. J. Doolan, "An experimental application of aeroacoustic time-reversal to the Aeolian tone," J. Acoust. Soc. Am. **139**(2), 740-763 (2016).

[23] T. J. Ulrich, P.A. Johnson, and A. Sutin, "Imaging nonlinear scatterers applying the time reversal mirror," J. Acoust. Soc. Am. **119**, 1514-1518 (2006).

[24] T. J. Ulrich, A. M. Sutin, R. A. Guyer, and P. A. Johnson, "Time reversal and nonlinear elastic wave spectroscopy TR NEWS techniques," Int. J. Nonlin. Mech. **43**, 209-216 (2008).

[25] B. E. Anderson, M. Griffa, T. J. Ulrich, P.-Y. Le Bas, R. A. Guyer, and P. A. Johnson, "Crack localization and characterization in solid media using time reversal techniques," Am. Rock Mech. Assoc., #10-154 (2010).

[26] M. Fink, "Time-reversed acoustics," Sci. Am. **281**(5), 91-97 (1999).

[27] P. C. de Mello, N. Pérez, J. C. Adamowski, and K. Nishimoto, "Wave focalization in a wave tank by using time reversal technique," Ocean Eng. **123**, 314-326 (2016).

[28] C. Heaton, B. E. Anderson, and S. M. Young, "Time reversal focusing of elastic waves in plates for educational demonstration purposes," J. Acoust. Soc. Am. **141**(2), 1084-1092 (2017).

[29] A. Derode, A. Tourin, and M. Fink, "Ultrasonic pulse compression with one-bit time reversal through multiple scattering," J. Appl. Phys. **85**(9), 6343–6352 (1999).

[30] G. Montaldo, P. Roux, A. Derode, C. Negreira, and M. Fink, "Generation of very high pressure pulses with 1-bit time reversal in a solid waveguide," J. Acoust. Soc. Am. **110**(6), 2849–2857 (2001).

[31] B. Van Damme, K. Van Den Abeele, Y. Li, and O. Bou Matar, "Time reversed acoustics techniques for elastic imaging in reverberant and nonreverberant media: An experimental study of the chaotic cavity transducer concept," J. Appl. Phys. **109**, 104910 (2011).

[32] B. E. Anderson, M. Clemens, and M. L. Willardson, "The effect of transducer directionality on time reversal focusing," J. Acoust. Soc. Am. **142**(1), EL95–El101 (2017).

[33] M. H. Denison and B. E. Anderson, "Time reversal acoustics applied to rooms of various reverberation times," J. Acoust. Soc. Am. **144**(6), 3055-3066 (2018).

[34] F. Fahy and P. Gardonio, Sound and Structural Vibration, Radiation, Transmission and Response, (Academic Press, Cambridge, MA, 2007), pp. 26, 185-195.

[35] A. Sutin, B. Libbey, V. Kurtenoks, D. Fenneman, and A. Sarvazyan, "Nonlinear detection of landmines using wide bandwidth time-reversal techniques," Proc. SPIE **6217**, 398–409 (2006).

[36] F. Ciampa and M. Meo, "Nonlinear elastic imaging using reciprocal time reversal and third order symmetry analysis," J. Acoust. Soc. Am. **131**(6), 4316–4323 (2012).